



EFFECT OF INTERFACE UNDULATIONS ON THE THERMAL FATIGUE OF THIN FILMS AND SCALES ON METAL SUBSTRATES

A. G. EVANS¹, M. Y. HE² and J. W. HUTCHINSON¹

¹Division of Engineering and Applied Sciences, Harvard University, Pierce Hall, Cambridge, MA 02138
and ²Department of Materials Engineering, University of California, Santa Barbara, CA 93106, U.S.A.

(Received 12 November 1996; accepted 28 January 1997)

Abstract—Oxide scales that form on superalloys eventually spall, especially upon thermal cycling. This phenomenon is motivated by the large residual *compression* in the oxide. Buckling and interface crack propagation are known aspects of this behavior, but the origin of the interface separation that precedes and activates buckling is not understood. One mechanism is described and analyzed in this article. It relies on the observation that the interfaces are typically non-planar. Such non-planarity can result in cyclic straining of the substrate, near the interface, leading to crack initiation by fatigue. The conditions that lead of cyclic plasticity are analyzed for a typical range of parameters. © 1997 Acta Metallurgica Inc.

1. INTRODUCTION

Thermally grown oxide thin films on metal alloy substrates are known to spall from the substrate upon thermal cycling, particularly Al₂O₃ on Ni or Fe-based alloys [1–4]. The oxide is typically in residual compression, caused primarily by the thermal expansion mismatch between the oxide film and the substrate. Recent measurements suggest that at room temperature these stresses are of the order of 3–5 GPa [5, 6]. In some cases, growth stresses are superposed, but they are relatively small. It has been surmised that these stresses motivate the spalling event. One key connection between the stresses and the spalling mechanism is addressed in this article.

It is established that large compressive stresses can cause buckling when an initial decohesion exists at the interface. The critical requirement for a circular decohesion is that its radius, b , satisfy [8]

$$b > 1.11h \sqrt{\frac{E_1}{(1 - \nu_1^2)\sigma}} \quad (1)$$

where σ is the residual compressive stress, h the film thickness, E_1 and ν_1 are the Young's modulus and Poisson's ratio of the film. Moreover, upon buckling, there is an energy release rate that can extend the crack and, thereby, cause spalling. The critical requirement for this to occur is expressible through a non-dimensional parameter [7]

$$\Omega = \frac{\sigma^2 h}{E_1 \Gamma_i} \quad (2)$$

where Γ_i is the interface toughness. For the buckled configuration to extend, it is required that Ω exceed a critical magnitude, Ω_c , of the order of 6 [8]. Often

the buckles propagate in a linear or “telephone cord” morphology [9] (see Fig. 1).

While the buckling and crack growth aspects of the spalling phenomenon are quite well understood, and experimentally validated [10] it is not known how the initial decohesions needed to satisfy the buckling condition (1) are created. Since the pre-existence of decohesions this large is unlikely, there have been various speculations about their formation, such as void formation and coalescence by diffusion [2, 11], but most of these are kinetic processes which occur at a rate governed primarily by the time spent at the highest temperature. The practical experience is that thermal cycling is often more important than prolonged isothermal exposure [12, 13]. The implication is that thermal fatigue is involved, embodied in cyclic plastic strains occurring either at the interface or in the substrate close to the interface. This realisation provides the basis for engineering models that characterise the cycles to failure, but a mechanistic basis has yet to be established. Such mechanism-based models are needed to identify the key variables and to understand scaling effects with those variables. The objective of this article is to provide a plausible cyclic mechanism with the associated analysis.

For a perfectly planar interface between the oxide and the substrate, there are no shear stresses along the interface, except near free edges and terminations [14–16]. Consequently, for typical thick substrates the yield condition can only be attained in these regions and spalls that occur remote from edges and features could not be explained. Thus, the idea that cyclic plastic strain at the interface could be important has been largely discounted. However, most interfaces

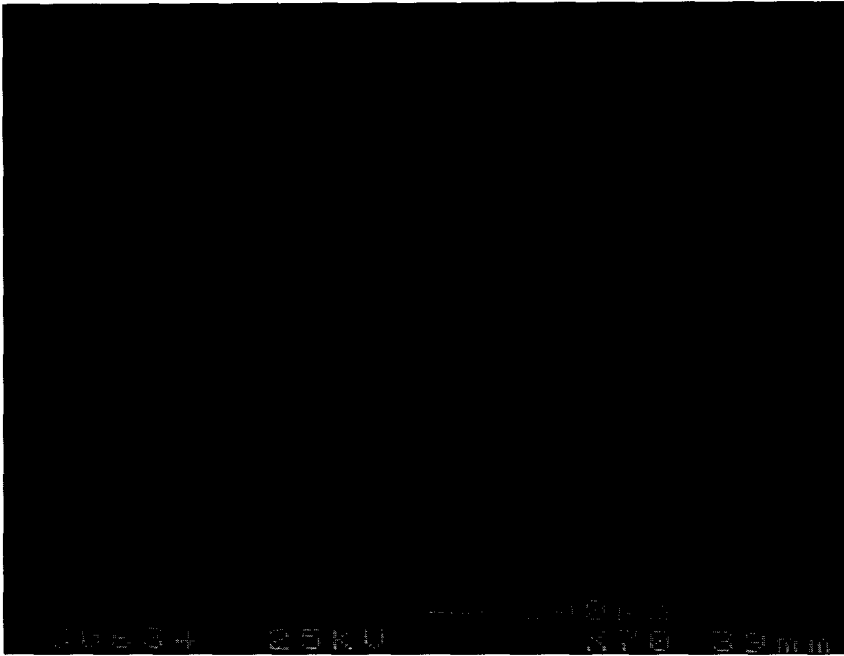


Fig. 1. A spalled region of an oxide scale formed at 1000°C on a Ni aluminide bond coat indicating the telephone cord morphology. The light grey areas are the spalled regions, while the dark grey areas are still attached (J. S. Wang, unpublished research).

with thermally grown oxides are non-planar, because of growth instabilities (Fig. 2) [17]. It will be shown that even small morphological perturbations from planarity have a surprisingly large effect on the stresses at the interface, as well as in the substrate. The conditions under which these stresses can induce cyclic plastic strains are analysed as a possible source of the initial interface decohesions that precede buckling. An elastic perturbation solution is presented first in order to elucidate trends and to identify the salient variables. These results are also used to estimate the plastic zone morphology and the shakedown conditions. Thereafter, detailed finite element results are obtained that embrace the full range of conditions expected in practice.

2. PERTURBATION SOLUTION

An elastically isotropic coating with Young's modulus E_1 , Poisson's ratio ν_1 and average thickness h is bonded to an infinitely deep substrate which is also isotropic with E_2 and ν_2 . The upper surface of the coating is assumed to be planar, but its interface with the substrate is wavy having amplitude A and wavelength L , varying according to $y = (A/2)\cos(2\pi x_1/L)$ (Fig. 3). The substrate/coating system is taken to be infinite in extent in the x_1 and x_3 directions. Gao [18] considered the same type of wavy interfaces, but for the case where both the substrate and the region above the interface are semi-infinite in extent in the direction perpendicular to the interface. Let T_0 be the temperature at which the coating is deposited on the substrate, and define ϵ_0^T to be the

thermal mismatch strain of the coating at any other temperature T as

$$\epsilon_0^T = \int_{T_0}^T (\alpha_1 - \alpha_2) dT \quad (3)$$

where α_1 and α_2 are the coefficients of thermal expansion of the coating and substrate. If the interface is planar ($A = 0$), the substrate is unstressed and two non-zero components of stress in the coating are

$$\sigma_{11}^0 = \sigma_{33}^0 = -\frac{E_1}{1 - \nu_1} \epsilon_0^T \equiv \sigma_0. \quad (4)$$

If the undulation amplitude A is non-zero, the stress and strain *changes* relative to the case with $A = 0$ satisfying the equations of plane strain. In what follows, a perturbation solution for the stresses and strains in the coating and substrate is given with A as the perturbation parameter. The solution, which is obtained to lowest order in A , will be seen to be reasonably accurate for surprisingly large non-planarities. It remains valid as long as the maximum slope of the interface, which is proportional to A/L , is not too large. There is no restriction on the magnitude of h/L . Denote components of stress, strain and displacement in the (x_1, x_2) plane using Greek subscripts in the standard manner, and write the perturbation expansion of the in-plane quantities according to

$$u_x = u_x^0 + A\tilde{u}_x + O(A^2)$$

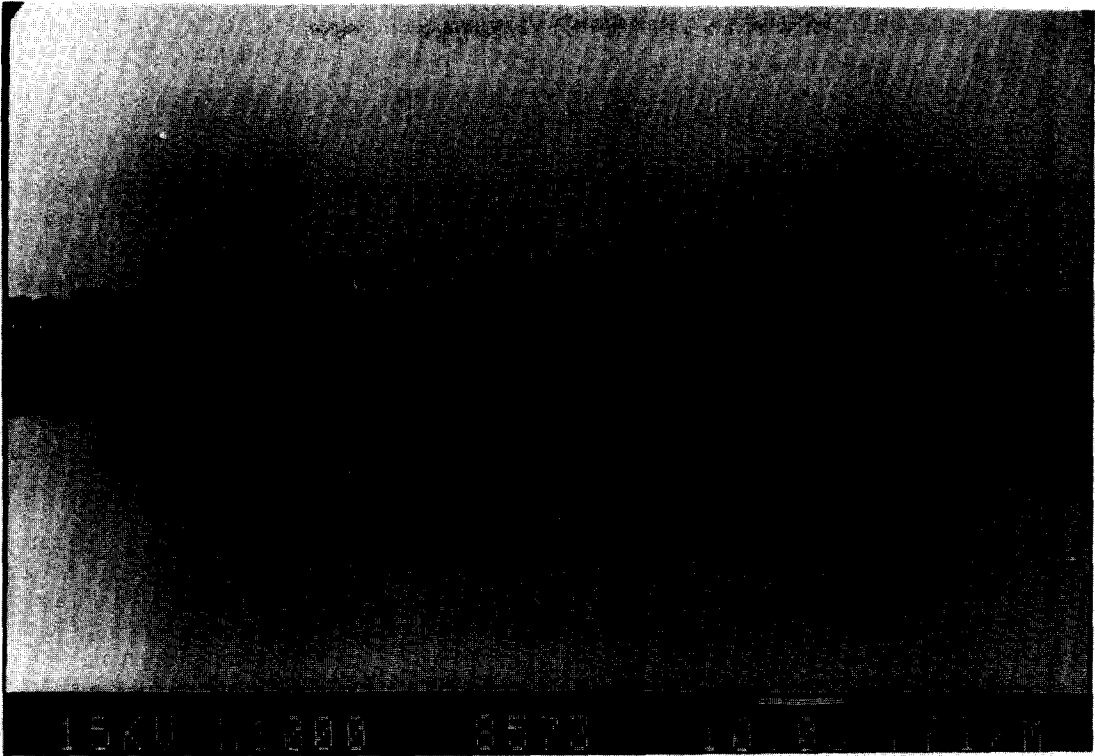


Fig. 2. Scanning electron microscopy of a double cross section of an alumina scale on an iron-based superalloy (FeAlCr) (M. Ruhle, unpublished research). The sections are attached by an epoxy bond (black). The dark grey regions are the oxide and the light grey the alloy. Note the undulations at the oxide/alloy interface and the protuberances into the alloy.

$$\begin{aligned} \epsilon_{\alpha\beta} &= \epsilon_{\alpha\beta}^0 + A\tilde{\epsilon}_{\alpha\beta} + O(A^2) \\ \sigma_{\alpha\beta} &= \sigma_{\alpha\beta}^0 + A\tilde{\sigma}_{\alpha\beta} + O(A^2). \end{aligned} \quad (5)$$

All the zeroth order quantities vanish in the substrate, while in the coating $\sigma_{12}^0 = \sigma_{22}^0 = 0$, σ_{11}^0 is given by equation (4), and

$$u_1^0 = 0, \quad u_2^0 = x_2 \epsilon_{22}^0, \quad \epsilon_{11}^0 = 0, \quad \epsilon_{22}^0 = \frac{(1 + \nu_1)}{(1 - \nu_1)} \epsilon_0^T. \quad (6)$$

The first order perturbations in equations (5) must satisfy equilibrium, $\tilde{\sigma}_{\alpha\beta,\beta} = 0$, the strain-displacement

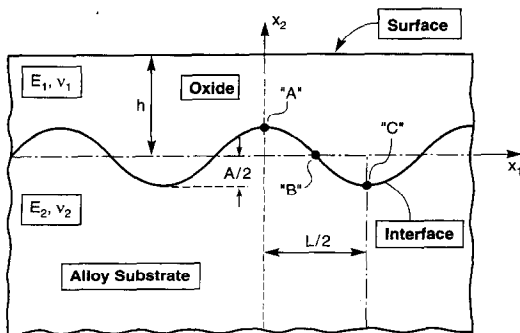


Fig. 3. A schematic of the configuration analysed, indicating the relevant parameters.

relations, $\tilde{\epsilon}_{\alpha\beta} = \frac{1}{2}(\tilde{u}_{\alpha,\beta} + \tilde{u}_{\beta,\alpha})$, and the plane strain stress and strain relations

$$\begin{aligned} \tilde{\sigma}_{\alpha\beta} &= \frac{E}{1 + \nu} \left(\tilde{\epsilon}_{\alpha\beta} + \frac{\nu}{1 - 2\nu} \tilde{\epsilon}_{\kappa\kappa} \delta_{\alpha\beta} \right) \\ \text{or } \tilde{\epsilon}_{\alpha\beta} &= \frac{1 + \nu}{E} (\tilde{\sigma}_{\alpha\beta} - \nu \tilde{\sigma}_{\kappa\kappa} \delta_{\alpha\beta}) \end{aligned} \quad (7)$$

with $(E, \nu) \equiv (E_1, \nu_1)$ in the coating and $(E, \nu) \equiv (E_2, \nu_2)$ in the substrate. Equilibrium is satisfied by stresses generated from an Airy stress function:

$$\tilde{\sigma}_{11} = \Phi_{,22}, \quad \tilde{\sigma}_{22} = \Phi_{,11}, \quad \tilde{\sigma}_{12} = -\Phi_{,12}. \quad (8)$$

Compatibility of the strains, with equation (7), requires that the Airy stress function satisfy

$$\nabla^4 \Phi = 0. \quad (9)$$

Continuity of displacements and tractions must be maintained across and along the wavy interface, $x_2 = y(x_1)$. It is these conditions which produce the non-homogeneous terms in the perturbation procedure. First, consider the continuity condition for displacements, $u_x^{(1)}(x_1, y(x_1)) = u_x^{(2)}(x_1, y(x_1))$, where superscripts (1) and (2) will be used to denote

quantities in the coating and substrate, respectively. From

$$u_x^{(\beta)}(x_1, y(x_1)) = u_x^{(\beta)}(x_1, 0) + \frac{\partial u_x^{(\beta)}}{\partial x_2}(x_1, 0)y(x_1) + \dots,$$

it follows from displacement continuity that

$$u_x^{(1)}(x_1, 0) - u_x^{(2)}(x_1, 0) = \left[\frac{\partial u_x^{(1)}}{\partial x_2}(x_1, 0) - \frac{\partial u_x^{(2)}}{\partial x_2}(x_1, 0) \right] y(x_1) + \dots \quad (10)$$

Conditions along the wavy interface are thereby replaced by conditions along $x_2 = 0$. When terms of the order of A are retained in these two equations after having been expressed in terms of the expansions (5), one obtains

$$\tilde{u}_1^{(1)}(x_1, 0) - \tilde{u}_1^{(2)}(x_1, 0) = 0$$

and

$$\tilde{u}_2^{(1)}(x_1, 0) - \tilde{u}_2^{(2)}(x_1, 0) = -\frac{1}{2} \epsilon_{22}^0 \cos(2\pi x_1/L). \quad (11a,b)$$

Similar treatment of traction continuity gives

$$\begin{aligned} \tilde{\sigma}_{12}^{(1)}(x_1, 0) - \tilde{\sigma}_{12}^{(2)}(x_1, 0) &= -(\pi/L)\sigma_{11}^0 \sin(2\pi x_1/L) \\ \text{and } \tilde{\sigma}_{22}^{(1)}(x_1, 0) - \tilde{\sigma}_{22}^{(2)}(x_1, 0) &= 0. \end{aligned} \quad (12a,b)$$

The Airy stress function will be used to generate the perturbation solution in each of the two regions. It is therefore expedient to obtain conditions equivalent to those in equations (11) and (12) expressed in terms of Φ . Conditions from equations (12a,b) follow immediately:

$$\begin{aligned} \Phi_{,12}^{(1)} - \Phi_{,12}^{(2)} &= (\pi/L)\sigma_{11}^0 \sin(2\pi x_1/L) \\ \text{and } \Phi_{,11}^{(1)} - \Phi_{,11}^{(2)} &= 0 \quad \text{on } x_2 = 0 \end{aligned} \quad (13a,b)$$

where $\Phi^{(1)}$ governs in $x_2 > 0$ and $\Phi^{(2)}$ in $x_2 < 0$. It is less straight forward to obtain replacements for equations (11a,b). It is useful at this juncture to anticipate the general result of Dundurs [19] which states that the inplane stresses, $\tilde{\sigma}_{\alpha\beta}$, can be expected to depend on the elastic mismatch between the coating and the substrate through only two mismatch parameters, α_D and β_D . For plane strain, the Dundurs mismatch parameters are

$$\begin{aligned} \alpha_D &= \frac{\bar{E}_1 - \bar{E}_2}{\bar{E}_1 + \bar{E}_2} \\ \text{and } \beta_D &= \frac{1}{2} \frac{\mu_1(1 - 2\nu_2) - \mu_2(1 - 2\nu_1)}{\mu_1(1 - \nu_2) + \mu_2(1 - \nu_1)} \end{aligned} \quad (14)$$

where $\bar{E} = E/(1 - \nu^2)$ and $\mu = E/(2(1 + \nu))$. The following steps are required to express equation (11a) in terms of Φ . Take the derivative of the equation with respect to x_1 ; note that $\tilde{u}_{1,1} = \tilde{\epsilon}_{11}$; express the strains in terms of stresses via equation (7); and express the stresses in terms of Φ via equation (8).

The final step is to make use of equation (14) and identities derived from equation (14), to arrive at

$$(1 - \alpha_D)\Phi_{,22}^{(1)} - (1 + \alpha_D)\Phi_{,22}^{(2)} + 2(\alpha_D - 2\beta_D)\Phi_{,11} = 0 \quad \text{on } x_2 = 0. \quad (15)$$

The first step in the reduction of equation (11b) starts with two derivatives of the equation with respect to x_1 , permitting displacement quantities to be replaced by strains. From this point on, the procedure parallels that just described, except in the final step when equation (13a) is used to eliminate the non-homogeneous term. The result is

$$\begin{aligned} (1 - \alpha_D)\Phi_{,112}^{(1)} - (1 + 5\alpha_D - 4\beta_D)\Phi_{,112}^{(2)} \\ + (1 - \alpha_D)\Phi_{,222}^{(1)} - (1 + \alpha_D)\Phi_{,222}^{(2)} = 0 \quad \text{on } x_2 = 0. \end{aligned} \quad (16)$$

The four continuity conditions are supplemented by the condition that the top surface of the coating is traction-free ($\Phi_{,11}^{(1)} = \Phi_{,12}^{(1)} = 0$ on $x_2 = h$) and the requirement that the stresses in the substrate decay to zero as $x_2 \rightarrow -\infty$. The system of equations admits a separable solution of the form

$$\begin{aligned} \Phi^{(1)} &= (\sigma_0/\lambda)f^{(1)}(x_2)\cos(2\pi x_1/L) \\ \text{and } \Phi^{(2)} &= (\sigma_0/\lambda)f^{(2)}(x_2)\cos(2\pi x_1/L) \end{aligned} \quad (17)$$

where $\lambda = 2\pi/L$. The general solution to equation (9) satisfying the traction-free condition on $x_2 = h$ and zero stress as $x_2 \rightarrow -\infty$ is

$$\begin{aligned} f^{(1)} &= a_1[\sinh \lambda(x_2 - h) - \lambda(x_2 - h)\cosh \lambda(x_2 - h)] \\ &\quad + a_2\lambda(x_2 - h)\sinh \lambda(x_2 - h) \\ f^{(2)} &= a_3e^{\lambda x_2} + a_4\lambda x_2 e^{\lambda x_2}. \end{aligned} \quad (18)$$

The four continuity conditions, (13a,b), (15) and (16), provide the equations for the four coefficients, a_i :

$$\sum_{j=1,4} M_{ij}a_j = b_i, (i = 1, 4) \quad (19)$$

where $b_1 = 1/2$ with $b_i = 0$ for $i = 2, 4$ and

$$\begin{aligned} M_{11} &= \lambda h S, \quad M_{12} = S + \lambda h C, \\ M_{13} &= 1, \quad M_{14} = 1, \\ M_{21} &= -S + \lambda h C, \quad M_{22} = \lambda h S, \\ M_{23} &= -1, \quad M_{24} = 0, \\ M_{31} &= (1 - \alpha_D)(S + \lambda h C), \\ M_{32} &= (1 - \alpha_D)(2C + \lambda h S), \\ M_{33} &= -1 - 3\alpha_D + 4\beta_D, \quad M_{34} = -2(1 + \alpha_D), \\ M_{41} &= -2(1 - \alpha_D)C, \quad M_{42} = -2(1 - \alpha_D)S, \\ M_{43} &= 4(\alpha_D - \beta_D), \quad M_{44} = -1 + 2\alpha_D - 4\beta_D \end{aligned} \quad (20)$$

with $S \equiv \sinh(\lambda h)$ and $C \equiv \cosh(\lambda h)$. Formulas for the a_i are too lengthy to be revealing, and, therefore, numerical solution of equation (19) is used to

generate results. Note that the a_i depend on the two Dundurs parameters and $\lambda h = 2\pi h/L$.

2.1. Stress at the interface in the substrate

The solution provides stresses to the order of A/L in the coating and in the substrate, for which the stresses vanish when $A = 0$. The emphasis here will be on the stresses in the substrate at the interface, which are given by

$$\begin{aligned} (\sigma_{11}, \sigma_{22}) &= \sigma_0 A \lambda \cos(2\pi x_1/L) (a_3 + 2a_4, -a_3), \\ \sigma_{12} &= \sigma_0 A \lambda \sin(2\pi x_1/L) (a_3 + a_4). \end{aligned} \quad (21)$$

The associated out-of-plane stress is $\sigma_{33} = \nu_2(\sigma_{11} + \sigma_{22})$, which brings in a dependence on ν_2 in addition to the Dundurs parameters. The von Mises effective stress in the substrate just below the interface is

$$\begin{aligned} \sigma_e &= \left\{ \frac{1}{2} [(\sigma_{11} - \sigma_{22})^2 + (\sigma_{11} - \sigma_{33})^2 \right. \\ &\quad \left. + (\sigma_{22} - \sigma_{33})^2] + 3\sigma_{12}^2 \right\}^{1/2} \\ &= |\sigma_0 A/L| \{ [Q_n \cos(2\pi x_1/L)]^2 \\ &\quad + [Q_s \sin(2\pi x_1/L)]^2 \}^{1/2} \end{aligned} \quad (22)$$

where

$$\begin{aligned} Q_n &= 2\pi \{ (1 - \nu_2 + \nu_2^2) [(a_3 + 2a_4)^2 + a_3^2] \\ &\quad + (1 + 2\nu_2 - 2\nu_2^2) a_3 (a_3 + 2a_4) \}^{1/2} \\ Q_s &= 2\pi \{ 3(a_3 + a_4)^2 \}^{1/2}. \end{aligned} \quad (23)$$

Note that $\sigma_e = |\sigma_0 A/L| Q_n$ is the effective stress in the substrate at the peaks and valleys of the interface undulation where the shear stress vanishes, while $\sigma_e = |\sigma_0 A/L| Q_s$ is the corresponding value at the midpoints where the maximum magnitude of the shear stress occurs and the normal components of stress vanish.

Plots of Q_n and Q_s as functions of α_D are given in Fig. 4 for five values of h/L with $\beta_D = \alpha_D/4$ and $\nu_2 = 0.3$. The dependence of these quantities on β_D was established by repeating the calculations with $\beta_D = 0$, which produces only small numerical changes from the results in Fig. 4. Since $0 < \beta_D < \alpha_D/4$ for most bi-material systems, it follows that β_D is of secondary importance. Similarly, the effect of ν_2 has been determined to be relatively small. More importantly, it can be seen that Q_n and Q_s are not only nearly equal, but they have little dependence on h/L over the probable range of interest for this parameter. It follows from these two observations that the von Mises effective stress in the substrate just below the interface is nearly independent of x_1 and can be approximated by

$$\sigma_e = |\sigma_0 A/L| Q(\alpha_D)$$

$$\text{where } Q \cong 3(1 - \alpha_D) - \frac{1}{2}(1 - \alpha_D)^2. \quad (24)$$

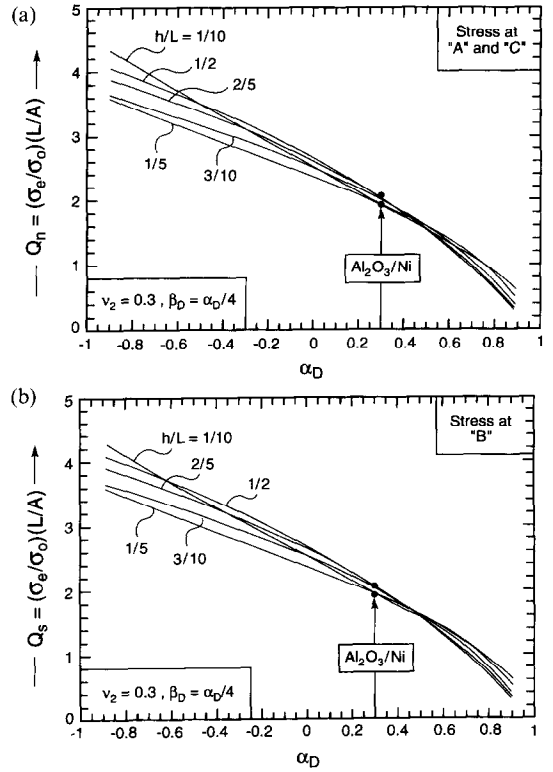


Fig. 4. Effect of the Dundurs parameter α_D on the non-dimensional factors in equation (22) for a range of normalized film thicknesses, h/L : ($\beta_D = \alpha_D/4$ and $\nu_2 = 0.3$): (a) Q_n (b) Q_s . (Note that there is little effect of the film thickness.) The α_D relevant to the $\text{Al}_2\text{O}_3/\text{Ni}$ system used for numerical analysis is indicated by the arrow.

2.2. Application of the perturbation solution to substrate yielding and shakedown

To provide a specific example, suppose the coating is deposited at T_0 and subsequently cooled to T . The thermal expansion mismatch, $\Delta\alpha = \alpha_1 - \alpha_2$, is imagined to be negative such that the thermal reference stress σ_0 in equation (4) is negative (compressive). In addition, to simplify the discussion, the yield strength of the substrate σ_Y will be assumed to be independent of temperature, but this restriction will be lifted in Section 3.

By equating σ_e to the yield strength of the substrate, the effect of the interface roughness on the incidence of substrate yielding can be estimated. By equation (24), the temperature drop at first yield corresponds to

$$\sigma_0 = -\frac{\sigma_Y}{Q(\alpha_D)} \left| \frac{L}{A} \right|. \quad (25)$$

Note that yielding is essentially independent of h/L , but there is a strong dependence on the elastic mismatch through α_D . Higher modulus films ($E_1 > E_2$ with positive α_D) decrease Q , but the effect is counteracted by the larger misfit stress as E_1 increases. There is an explicit inverse dependence on

the relative amplitude of the interface undulations, A/L . These trends are used to establish the scope of selected numerical calculations presented in Section 3.

Upon thermal cycling with amplitude $\Delta T = T_0 - T$, it can be asserted that some plastic straining will occur in each cycle if the *change* $\Delta\sigma_e$ in the effective stress, due to ΔT , exceeds $2\sigma_Y$ predicted by an elastic analysis [20]. Elastic shakedown is only possible if $\Delta\sigma_e \leq 2\sigma_Y$. In Section 3 it will be established that the shakedown limit for coating/substrate systems is well approximated by the condition $\Delta\sigma_e = 2\sigma_Y$. Based on the perturbation result (4), the shakedown condition for the idealized case of a temperature-independent substrate yield stress is therefore that ΔT be

$$-\sigma_0 \leq \frac{2\sigma_Y}{Q(\alpha_D)} \left| \frac{L}{A} \right|. \quad (26)$$

The significance of equation (26) is that, when satisfied, the substrate response becomes elastic after the first cycle. Consequently, there can be no fatigue, rendering this mechanism incapable of creating initial decohesions at the interface. Condition (26) thus becomes a benchmark for ascertaining the thermal range, ΔT , and roughness amplitude, A/L , above which thermal fatigue can be anticipated.

3. NUMERICAL RESULTS

The numerical calculations are performed for a thin film on a very thick substrate, so that bending of the substrate is excluded. Symmetry permits a unit cell of width $L/2$ to be analysed, extending from $x_1 = 0$ to $L/2$ in Fig. 3, with periodic boundary conditions imposed. A finite element mesh designed to resolve the stresses near the coating/substrate interface was used in carrying out the calculations. A difference in thermal expansion coefficient, $\Delta\alpha = \alpha_1 - \alpha_2$, between the film and substrate is imposed. In the numerical calculations, the elastic properties are chosen to represent Al_2O_3 on Ni alloys (Table 1), such that the Dundurs' parameters are: $\alpha_D = 0.31$ and $\beta_D = 0.06$. The Poisson's ratio in the substrate is $\nu_2 = 0.3$. The film thickness is kept constant at $h/L = 1$, since the preceding analytical results have indicated that this dimension has only a second order influence on the stresses. (Selected numerical results for smaller values of h/L were obtained to further verify this assertion.)

Elastic calculations of the effective stress in the substrate have been made at the point where it is largest (point "A" in Fig. 3, just below the interface

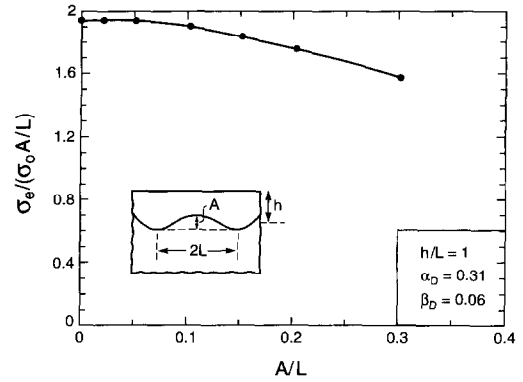


Fig. 5. Dependence of normalized effective stress at point "A" determined from an elastic computation, as a function of A/L . Note the extensive range of accuracy of the perturbation solution. Compare the results as $A \rightarrow 0$ with the analytic results for $\alpha_D = 0.31$ from Fig. 4.

at $x_1 = 0$) as a function of A/L . The solution depends linearly on the reference stress σ_0 in equation (4). The result is normalized in a way that brings out the accuracy of the perturbation solution. The numerical results (Fig. 5) approach the perturbation result as A/L becomes small, evident upon comparing the asymptote $A/L \rightarrow 0$ with Q_s or Q_n from Figs 4(a) and (b) (for $\alpha_D = 0.31$). This consistency provides a check on the accuracy of the finite element model. Moreover, the two sets of results continue to approximate each other reasonably well, even for undulation amplitudes as large as $A/L = 0.3$.

Contours corresponding to constant values of effective stress in the substrate as computed by the finite element model, assuming that the *substrate remains elastic*, are displayed in Fig. 6 for three values of A/L . The significance of these stress levels can be appreciated by noting that σ_0 for the $\text{Al}_2\text{O}_3/\text{Ni}$ system at room temperature is about -3 GPa [6]. At the smallest undulation amplitude, $A/L = 0.1$, the contour of constant effective stress is almost parallel to the interface in close accord with the approximate perturbation result in equation (24). This characteristic is attributed to the largely deviatoric nature of the deformations arising at all locations along the interface. That is, at the peaks and valleys of the undulations (points "A" and "C" in Fig. 3), yielding is encouraged by a combination of either tensile σ_{11} and compressive σ_{22} stresses, or vice versa, while at the mid-position (point "B"), shear stresses σ_{12} are dominant. Some variation of σ_e along the interface becomes apparent at $A/L = 0.3$. The largest value is attained just below the interface at the peak of the undulation (point "A"), and the smallest value at point "B". The effective stress at the valley of the undulation (point "C") is intermediate between the other two values. These trends are further emphasised at the largest amplitude shown, $A/L = 0.5$. It is apparent from this numerical example that effective stresses, large enough to produce plastic staining in the substrate, must be expected when interface

Table 1. Material properties summary

Material	E (GPa)	ν	α ($10^{-6} \text{ } ^\circ\text{C}^{-1}$)
Al_2O_3	400	0.2	8
Ni alloy	200	0.3	15

undulations are not tightly controlled. By this example and the results in Fig. 5, it has also been demonstrated that the perturbation results can be used with confidence to predict elastic stresses for undulation amplitudes as large as about $A/L = 0.3$.

3.1. Temperature-independent yield strength

To establish limits on temperature variations corresponding to initial plastic yielding and to elastic shakedown for thermal cycling, an elastic-perfectly plastic substrate with a temperature-independent yield strength, σ_Y , is considered first. The following history is prescribed in accordance with the notation in Fig. 7, which depicts the effective stress variation at a point in the substrate such as "A". The coating is assumed to be deposited stress-free at temperature T_0 . The temperature T is then lowered to $T_4 \equiv RT_0$, generating a compressive thermal reference stress σ_0 defined in equations (3) and (4). The results presented below in terms of σ_0 do not require that the mismatch in the coefficients of thermal expansion be temperature independent, but when it is,

$$\sigma_0 = -\frac{E_1 \Delta \alpha (T_4 - T_0)}{(1 - \nu_1)} \quad (27)$$

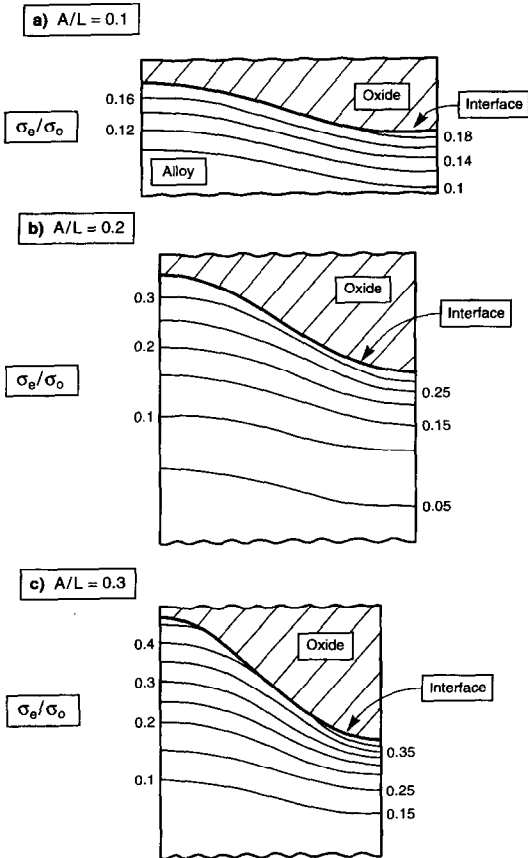


Fig. 6. Equivalent stress contours in the substrate at three undulation amplitudes as determined by an elastic analysis using the finite element model ($\alpha_D = 0.31$, $\beta_D = 0.06$, $\nu_2 = 0.3$, $h/L = 1$).

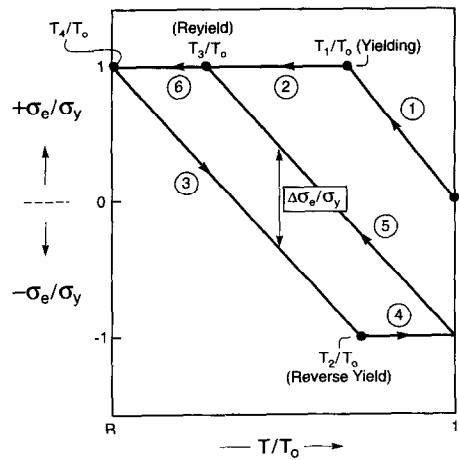


Fig. 7. History of effective stress at a point such as "A" in an elastic-perfectly plastic substrate with a temperature-independent yield strength σ_Y . The film/substrate system is subject to a temperature history with cycles from T_0 to T_4 , where the initial stress is taken to be zero at the start of the history at T_0 . The case illustrated involves plastic straining in each cycle. For the purposes of displaying the effective stress history it is convenient to plot the variation by changing the sign of σ_e at each T where it becomes zero, in the manner illustrated here. This reflects the fact that individual components of stress change sign when T is varying monotonically and σ_e vanishes.

At this point the temperature is raised back to T_0 , and the temperature history is repeated, cycling between T_0 and T_4 . The same two questions examined in Section 2.2 are first readdressed here: (i) Is R sufficiently large that no plastic yielding occurs in the entire history? (ii) If not, is R in the range such that plastic deformation occurs in the first few cycles but subsequently shakes down with only an incremental elastic response (i.e. the hysteresis loop, $3 \rightarrow 4 \rightarrow 5 \rightarrow 6 \rightarrow 3$, in Fig. 7 has zero width)?

Results of the numerical calculations are shown in Fig. 8 for the elastic-perfectly plastic substrate with a temperature independent yield strength σ_Y . The solid line curve labelled "initial yielding" corresponds to the largest magnitude of σ_0 such that no yielding occurs during the thermal history at a given undulation amplitude A/L . The solid line labelled "elastic shakedown" represents the largest magnitude of σ_0 at a given A/L such that after one or more thermal cycles, no subsequent plastic yielding occurs. Note that the shakedown reference stress is approximately twice the reference stress at initial yield. Moreover, the predictions based on the perturbation analysis, equations (25) and (26), which are plotted as dashed curves, provide a good approximation to the numerical results even at interface undulation amplitudes as large as $A/L = 0.3$. With due account for the temperature dependence of σ_Y , the results from the perturbation analysis can be used to establish conditions on the thermal cycles which ensure shakedown.

When σ_0 lies between the curves labelled “initial yield” and “elastic shakedown” in Fig. 8, plastic yielding occurs as the temperature drops toward T_4 , but upon reheating to T_0 , there is no reverse yielding and the substrate experiences only elastic deformation in the subsequent thermal cycles. When σ_0 lies above the elastic shakedown threshold, reversed plastic flow occurs in the first cycle as the temperature is brought back up to T_0 . Figure 9 displays the active plastic zones in the *first cycle*, at $T = T_4$ and then at the end of the cycle at $T = T_0$. After one or more subsequent cycles, plastic straining settles down to steady hysteretic behavior, as illustrated by two sets of numerical results in Fig. 10 for ϵ_{22}^p at “A”. Included in Fig. 8(b) are curves associated with two levels of effective plastic strain increment,

$$\Delta \epsilon_c^p = \int_{T_2}^{T_0} \sqrt{\frac{2}{3} \dot{\epsilon}_{ij}^p \dot{\epsilon}_{ij}^p}, \quad (28)$$

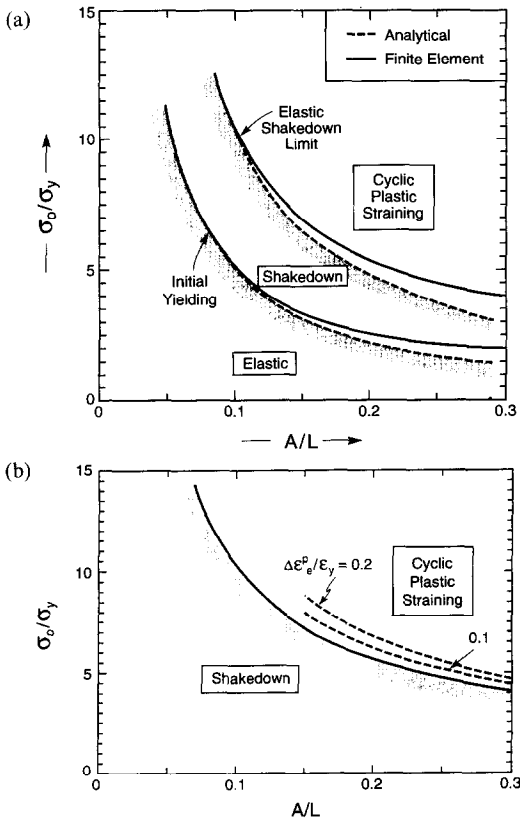


Fig. 8. Thermal fatigue maps characterising the regions in which initial yielding, shakedown and cyclic plasticity occur. The ordinate is the ratio of the reference thermal stress to the substrate yield strength and the abscissa is the ratio of the amplitude to the wavelength of the roughness, A/L . (a) Estimates obtained from the perturbation analysis (dashed curves) and from the finite element analysis (solid curves) are both shown. (b) Above the shakedown threshold, curves corresponding to specified effective plastic strain amplitudes characterizing the width of the hysteresis loop are also plotted, as obtained from the numerical calculations. The yield strength is independent of temperature, $\alpha_D = 0.31$, $\beta_D = 0.06$, $\nu_2 = 0.3$ and $h/L = 1$.

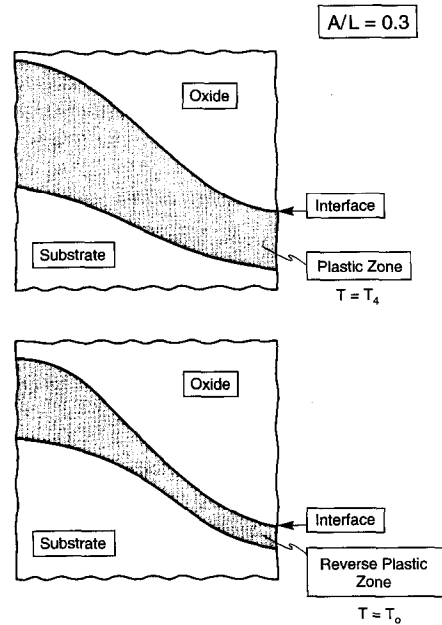


Fig. 9. Typical active plastic zones in the first thermal cycle from the numerical calculations when σ_0 exceeds the shakedown threshold. (a) Initial zone on cooling to T_4 ; (b) reverse plastic zone on reheating to T_0 . The results correspond to $\sigma_0/\sigma_Y = 7$. The temperature T_4 and T_0 are defined in Fig. 7.

normalized by the elastic yield strain $\epsilon_Y = \sigma_Y/E_2$. This measure characterizes the width of the cyclic hysteresis loop (c.f. Figs 7 and 10) when σ_0 exceeds the shakedown threshold. The values in equation (28) were calculated at point “A”, but the equivalent stresses and strains calculated at this location closely represent the behavior found at all other locations along the interface. Thermal fatigue is expected to be related to the level of reversed plastic strain per cycle in the substrate at the interface if this is the operative mechanism.

3.2. An example for a substrate with a temperature-dependent yield strength

The yield strength of the substrate can vary significantly over the temperature cycle, as illustrated by data for a superalloy and an intermetallic in Fig. 11 [21]. To illustrate how such temperature-dependent yielding affects the deformation history of the substrate, numerical computations have been carried out for a hypothetical case where the substrate is again elastic–perfectly plastic with $\sigma_Y(T)$ varying linearly from 700 MPa at 0°C to 220 MPa at 1000°C . The other properties of the film and the substrate are temperature-independent and taken to be the same as those used in the previous sub-section. The imposed temperature variation starts at $T = 1000^\circ\text{C}$, where the stress in the substrate is assumed to be zero, and is subsequently cycled between 0 and 1000°C . The effective stress history at point “A” is plotted in Fig. 12(a) in the same manner

as for the earlier case. Now, as the temperature drops and yielding occurs, the effective stress increases in accordance with the temperature-dependent yield stress. As the temperature reverses in the second half of the cycle, the opposite happens. The history of the dominant plastic strain component at "A" is displayed in Fig. 12(b). After the first cycle, a steady hysteresis sets in with reversed plastic straining in each cycle.

4. SOME USEFUL APPROXIMATIONS

The preceding results suggest approximations that might be used for the development of a mechanism-based life prediction methodology. The underlying principles are illustrated by graphical presentations which commence with the construction of Fig. 13. Let T_U and T_L denote the upper and lower limits, respectively, of the repeated temperature cycle. Plot the curves for the substrate yield strength, $\pm\sigma_Y(T)$, over this temperature range. Attention will focus on whether or not cyclic plastic straining occurs, and not

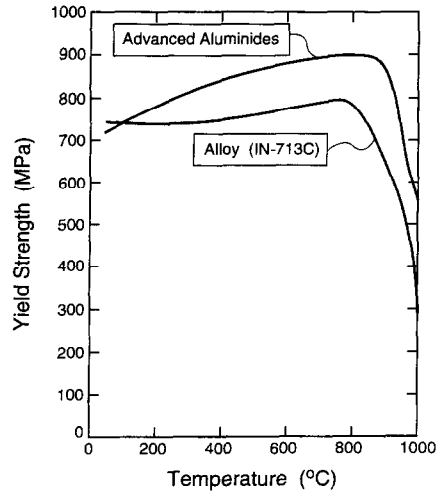


Fig. 11. Temperature dependence of yield strength for a typical superalloy, as well as for an intermetallic that might be used as bond coat.

on the less important issue of initial yield following coating or scale growth. It should be evident from the two previous numerical examples that development of a steady hysteresis cycle is tied to T_U and T_L and not the deposition temperature, T_0 , which need not coincide with T_L . Construct the hysteresis loop in

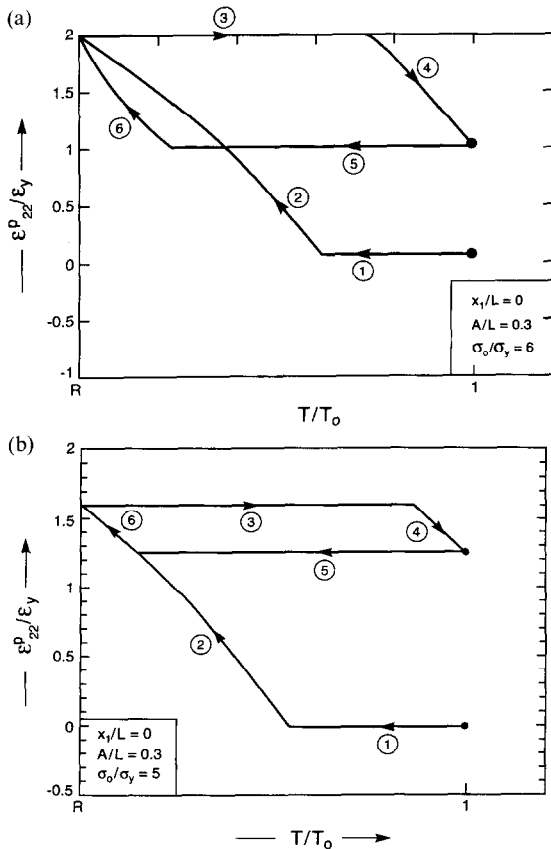


Fig. 10. The history of the plastic strain component, ϵ_2^p , at point "A". The segments of the history are numbered to correspond with the numbering in Fig. 7. Beyond the first cycle, the history of ϵ_2^p repeats itself. Similar plots pertain to other plastic strain components and to other locations. The results have been computed for the case: (a) $\sigma_0/\sigma_y = 6$ and (b) $\sigma_0/\sigma_y = 5$.

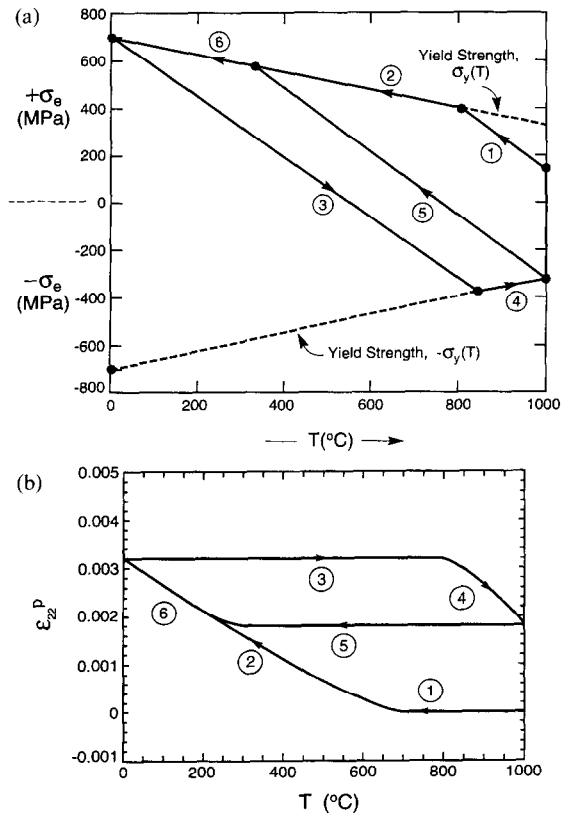


Fig. 12. A numerical example illustrating the effect of a temperature-dependent substrate yield strength. (a) Effective stress history, and (b) history of ϵ_2^p at point "A".

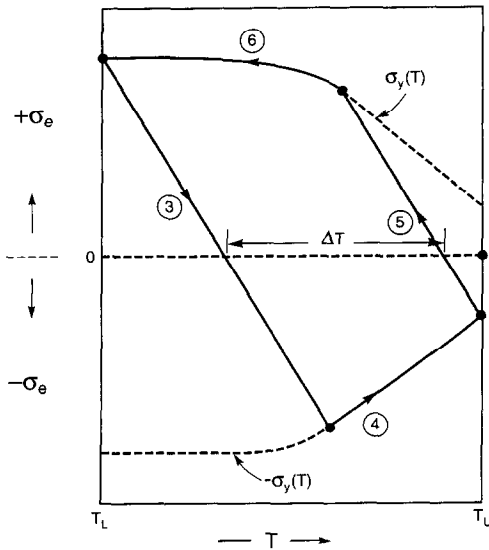


Fig. 13. Plot of effective stress history at the interface in the substrate in steady thermal cycling between T_U and T_L for an elastic-perfectly-plastic substrate with a temperature-dependent yield strength. The width of the loop, ΔT , is taken at the axis $\sigma_e = 0$, as shown.

Fig. 13 by drawing line #3 starting at $\sigma_y(T_L)$. In this segment of the cycle the response of the substrate is elastic, and thus, from equation (24), the slope of the line is well approximated by

$$\frac{d\sigma_e}{dT} = - \left| \frac{E_1 \Delta \alpha}{(1 - \nu_1)} \frac{A}{L} \right| Q(\alpha_D). \quad (29)$$

In plotting Fig. 13, the mismatch in thermal expansion coefficients was taken to be independent of temperature, such that line #3 is straight. In a similar manner, draw in line #5 starting at $-\sigma_y(T_U)$, also with slope (29). The case depicted in Fig. 13 illustrates a history with reversed plastic straining in each cycle. If it had been the case that

$$\left| \frac{E_1 \Delta \alpha}{(1 - \nu_1)} \frac{A}{L} \right| Q(\alpha_D) [T_U - T_L] < [\sigma_y(T_U) + \sigma_y(T_L)], \quad (30)$$

then the loop would have zero width and elastic shakedown would pertain.

If elastic shakedown is not predicted, it is expected that the fatigue life of the coating will depend on the level of the plastic straining (28) in each thermal cycle at the interface in the substrate. Insight into the magnitude of plastic strains occurring in each cycle when the shakedown limit (30) is exceeded can be obtained from an understanding of the stresses and strains which develop along the interface in an elastic cycle. Were no tractions to be exerted by the substrate on the coating (away from the substrate edges), equilibrium would result in higher inplane stress and strain where the coating is thinner. The film would

clearly undergo in-plane straining incompatible with the substrate. The stresses and strains which develop at the interface in the substrate arise to enforce strain compatibility and to counteract the force imbalance in the coating. The shear traction on the interface is largest midway between the peaks and valleys of the interface undulation, alternating in sign so as to consistently stretch or compress the respective thin and thick sections of the coating. The normal traction attains the largest magnitude at the peaks and valleys of the undulation, also alternating in sign. Plastic deformation at the interface in the substrate tends to relax the requirement of local in-plane strain compatibility between the coating and the substrate. It is to be expected, therefore, that the plastic strain induced once yielding starts should be of the order of the elastic strain which would otherwise occur.

An approximate expression for the width of the plastic hysteresis loop, $\Delta \epsilon_e^p$, is developed based on the above reasoning. Consider first substrates with a temperature-independent yield strength. Let $\Delta \sigma_0$ denote the change in the thermal reference stress (4) occurring after the yield in the substrate starts in any cycle. That is, if $\Delta \alpha$ is temperature-independent and ΔT denotes the width of the loop in a plot such as Fig. 13, then

$$\Delta \sigma_0 = \frac{E_1 \Delta \alpha \Delta T}{(1 - \nu_1)}. \quad (31)$$

Using equation (24) to estimate the associated increment in the effective strain, $(\Delta \epsilon_e)_{\text{elastic}}$, as predicted by an elastic analysis, gives i.e.

$$(\Delta \epsilon_e)_{\text{elastic}} = \left| \frac{\Delta \sigma_0}{E_2} \frac{A}{L} \right| Q. \quad (32)$$

As an approximation, the effective plastic strain increment $\Delta \epsilon_e^p$ can be expressed as

$$\frac{\Delta \epsilon_e^p}{(\Delta \epsilon_e)_{\text{elastic}}} = F \left[\frac{(\Delta \epsilon_e)_{\text{elastic}}}{\epsilon_Y} \right] \quad (33)$$

where F is a function. Numerical results for $\Delta \epsilon_e^p$ from the finite element calculations for substrates with a temperature-independent yield stress are plotted in this manner in Fig. 14. The function

$$F(x) = 1.32x - 0.668x^2 + 0.123x^3 \quad (34)$$

gives a good fit to the data for $A/L = 0.3$ over the range plotted. The formula (33) clearly fails to capture the full A/L dependence, but in conjunction with equation (34) should provide a useful approximation. Any formula such as equation (33) must necessarily over-simplify the cyclic plastic strain dependencies. In a given cycle, yielding starts at point "A" and spreads along the interface. Formula (33) reflects the fact that there will be more constraint to plastic flow when $(\Delta \epsilon_e)_{\text{elastic}}/\epsilon_Y$ is small than when it is of order unity with yielding occurring all along the interface.

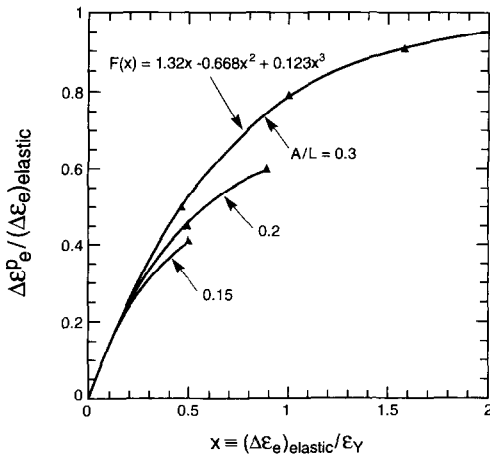


Fig. 14. Selected numerical results for the width of the hysteresis loop as measured by $\Delta\epsilon_e^p$ and the function $F(\cdot)$ in equation (33).

Accurate prediction of $\Delta\epsilon_e^p$ for substrates with *temperature-dependent yielding* will require further research. In the interim, the following approach based on equation (33) is suggested. Two additional complications now arise in using equation (33) to predict $\Delta\epsilon_e^p$: (i) the temperature increment ΔT during which yield occurs differs for the heating and cooling segments of the cycle (c.f. Fig. 13); and (ii) ϵ_Y depends on T . With ΔT identified as shown in Fig. 13, the largest estimate of $\Delta\epsilon_e^p$ from equation (33) would be obtained with $\epsilon_Y = \epsilon_Y(T_U)$, while the smallest estimate would be obtained using $\epsilon_Y = \epsilon_Y(T_L)$. These values should bracket $\Delta\epsilon_e^p$, subject to the accuracy of equation (33) itself. In a steady cyclic hysteresis loop, the effective plastic strain increment must be the same for the heating and cooling segments. This suggests that the average of the two estimates may be a reasonable choice, i.e.

$$\frac{\Delta\epsilon_e^p}{(\Delta\epsilon_e)_{\text{elastic}}} = \frac{1}{2} \left\{ F \left[\frac{(\Delta\epsilon_e)_{\text{elastic}}}{\epsilon_Y(T_U)} \right] + F \left[\frac{(\Delta\epsilon_e)_{\text{elastic}}}{\epsilon_Y(T_L)} \right] \right\}. \quad (35)$$

5. IMPLICATIONS AND CONCLUSIONS

The results identify explicit ranges in material properties that separate shakedown from cyclic plastic straining. The principal factors are the thermal expansion misfit between the scale and the substrate, $\Delta\alpha$, the scale modulus, E , the substrate yield strength, σ_Y , the cyclic temperature range, ΔT , and the amplitude, A , of the undulations that develop at the scale/substrate interface. The thickness of the scale, h , has only a secondary importance. The effects of $\Delta\alpha$, ΔT , E and σ_Y are consistent with engineering models and practical experience. The roles of A and h require some discussion. While h increases with dwell time at high temperature, this thickening has little effect on the thermal fatigue, so that there is no obvious role of the dwell, in apparent contradiction with the

practical findings. However, the interfaces also change with dwell time, usually developing larger amplitude undulations as the scale thickens. This effect of time on A could be the source of the dwell time effect. The reasons for changes occurring in A as the scale develops are not well-documented, but will be addressed in future research.

One way in which the above results can be used to understand the initial stages of spalling once cyclic plastic straining commences is to relate $\Delta\epsilon_e^p$ to the number of reversals needed to initiate fatigue, designated N_i . For this purpose, the Coffin–Manson relation [22, 23] is assumed to apply:

$$N_i = (1/2)(\Delta\epsilon_e^p/2\epsilon_r)^{1/c} \quad (36)$$

where ϵ_r is a ductility measure that calibrates the behavior and the exponent c is in the range -0.5 to -0.7 . Combining equations (31)–(34) with equation (36) gives

$$N_i = (1/2) \left[\frac{E_1 \Delta\alpha \Delta T A}{2E_2 \epsilon_r (1-\nu)L} Q \right]^{1/c} F^{1/c} \quad (37)$$

where it is recalled that ΔT denotes the width of the hysteresis loop as identified in Fig. 13. This result contains parameters that can be verified and experimentally tested in order to evaluate the importance of cyclic plasticity in the initiation of interface separations. Such evaluations are in progress. However, as noted above, a full life prediction model would need to include the subsequent buckling and buckle propagation, as well as possible high temperature interface crack initiation and growth processes.

Acknowledgements—This work was supported in part by the DARPA University Research Initiative through grant N00014-92-J-1808, by the NSF through grant DMR-94-00396 and by the Division of Engineering and Applied Sciences at Harvard University.

REFERENCES

1. Miller, R. A., *Thin Solid Films*, 1982, **95**, 265.
2. Meier, S. M., Nissley, D. M., Sheffler, K. D. and Cruse, T. A., *J. Engng Gas Turbines and Power*, 1992, **114**, 258.
3. Sheffler, K. D. and Gupta, D. K., *J. Engng Gas Turbines and Power*, 1988, **110**, 605.
4. Brindley, W. J. and Miller, R. A., *Surf. Coat. Technol.*, 1990, **43**, 446.
5. Christensen, R. J., Lipkin, D. M. and Clarke, D. R., *Appl. Phys. Lett.*, 1996, **69**, 3754.
6. Lipkin, D. M. and Clarke, D. R., *Oxidation of Metals*, 1996, **34**, 125.
7. Evans, A. G. and Hutchinson, J. W., *Acta metall. mater.*, 1995, **43**, 2507.
8. Hutchinson, J. W. and Suo, Z., *Adv. Appl. Mech.*, 1992, **29**, 63.
9. Hutchinson, J. W., Thouless, M. D. and Liniger, E. G., *Acta metall. mater.*, 1992, **40**, 295.
10. Thouless, M. D., Jensen, H. M. and Liniger, E. G., *Proc. R. Soc., London*, 1994, **A447**, 271.
11. Evans, A. G., Crumley, G. B. and Demaray, R. E., *Oxidation and Metals*, 1983, **20**, 193.

- | | | |
|--|-------------------|---|
| 12. Wright, K., 1996, unpublished research at General Electric. | b | critical radius for buckling |
| 13. Miller, R. A., <i>J. Am. Ceram. Soc.</i> , 1984, 67 , 517. | C | cosh (λh) |
| 14. Chen, K. S., He, M. Y. and Hutchinson, J. W., <i>Mater. Sci. Engng</i> , 1993, A167 , 57. | E | Young's modulus |
| 15. Bak, M. and Koenig, H. A., <i>Engng Fracture Mech.</i> , 1994, 48 , 583. | F | function [see equation (34)] |
| 16. Kuo, A. Y., <i>J. appl. Mech.</i> , 1978, 56 , 585. | h | film thickness |
| 17. Ruhle, M., 1996, unpublished research at Max Planck Institut, Stuttgart. | L | undulation wavelength |
| 18. Gao, H., <i>Int. J. Solids Struct.</i> , 1991, 28 , 703. | N_i | number of cycles |
| 19. Dundurs, J., <i>J. appl. Mech.</i> , 1969, 36 , 650. | Q | stress scaling coefficient |
| 20. Drucker, D. C. and Palgen, L., <i>J. appl. Mech.</i> , 1981, 48 , 479. | S | sinh (λh) |
| 21. Liu, C. T. and White, C. L., <i>High Temperature Ordered Intermetallic Alloys</i> , Materials Research Society, 1985, 39 , 365. | T | temperature |
| 22. Coffin, L. F., <i>Trans. ASME</i> , 1954, 76 , 931. | u_i | displacements |
| 23. Manson, S. S., National Advisory Commission on Aeronautics, Report 1170, Cleveland Lewis Propulsion Laboratory, 1954. | u_i^0 | displacements in film |
| | x_i | coordinate |
| | α | thermal expansion coefficient |
| | α_D | Dundur's parameter [see equation (14)] |
| | β_D | Dundur's parameter |
| | ϵ_y | yield strain |
| | ϵ_0^T | thermal misfit strain |
| | ϵ_{ij}^0 | strains in film |
| | ϵ_{ij}^p | plastic strain |
| | Γ_i | interface toughness |
| | ν | Poisson's ratio |
| | λ | $2\pi/L$ |
| | σ | residual compressive stress |
| | σ_{ij}^0 | stresses in film |
| | σ_0 | misfit stress [see equation (4)] |
| | σ_e | equivalent stress [see equation (22)] |
| | σ_y | yield strength of substrate |
| | Ω | cracking coefficient [see equation (2)] |

APPENDIX

Nomenclature

A undulation amplitude